Journal of Microbiology (2021) Vol. 59, No. 2, pp. 142–150
DOI 10.1007/s12275-021-0441-0
eISSN 1976-3794
pISSN 1225-8873

iTRAQ-facilitated proteomic analysis of *Bacillus cereus* via degradation of malachite green[§]

Bobo Wang[1], Jing Lu[1], Junfang Zheng[2], and Zhisheng Yu[1]*

[1]*College of Resources and Environment, University of Chinese Academy of Sciences, Beijing 100049, P. R. China*
[2]*Department of Biochemistry and Molecular Biology, School of Basic Medical Sciences, Capital Medical University, Beijing 100069, P. R. China*

(Received Aug 24, 2020 / Revised Nov 30, 2020 / Accepted Dec 1, 2020)

The wide use of malachite green (MG) as a dye has caused substantial concern owing to its toxicity. *Bacillus cereus* can against the toxic effect of MG and efficiently decolourise it. However, detailed information regarding its underlying adaptation and degradation mechanisms based on proteomic data is scarce. In this study, the isobaric tags for relative and absolute quantitation (iTRAQ)-facilitated quantitative method was applied to analyse the molecular mechanisms by which *B. cereus* degrades MG. Based on this analysis, 209 upregulated proteins and 198 downregulated proteins were identified with a false discovery rate of 1% or less during MG biodegradation. Gene ontology and KEGG analysis determined that the differentially expressed proteins were enriched in metabolic processes, catalytic activity, antioxidant activity, and responses to stimuli. Furthermore, real-time qPCR was utilised to further confirm the regulated proteins involved in benzoate degradation. The proteins BCE_4076 (Acetyl-CoA acetyltransferase), BCE_5143 (Acetyl-CoA acetyltransferase), BCE_5144 (3-hydroxyacyl-CoA dehydrogenase), BCE_4651 (Enoyl-CoA hydratase), and BCE_5474 (3-hydroxyacyl-CoA dehydrogenase) involved in the benzoate degradation pathway may play an important role in the biodegradation of MG by *B. cereus*. The results of this study not only provide a comprehensive view of proteomic changes in *B. cereus* upon MG loading but also shed light on the mechanism underlying MG biodegradation by *B. cereus*.

***Keywords*:** iTRAQ, proteomic, *Bacillus cereus*, malachite green, biodegradation

*For correspondence. E-mail: yuzs@ucas.ac.cn; Tel.: +86-10-88256057; Fax: +86-10-88256057
[§]Supplemental material for this article may be found at http://www.springerlink.com/content/120956.

Introduction

Malachite green (MG) is a water-soluble triarylmethane dye. It is widely used in several industries, including the dyeing, printing, aquaculture, and pharmaceutical industries (Henderson *et al.*, 1997; Moumeni and Hamdaoui, 2012; Saha *et al.*, 2012). Therefore, MG is often detected in many aquatic products and industrial wastewater. The abuse of MG has attracted substantial attention owing to its toxic effects. It is reported that MG can cause respiratory toxicity, carcinogenesis, mutagenesis, teratogenicity, and chromosomal fractures (Zhang *et al.*, 2013). Mutagenic effects, organ damage, and developmental abnormalities have been observed in higher eukaryotes (Fessard *et al.*, 1999; Srivastava *et al.*, 2004). Therefore, pollution caused by MG cannot be neglected.

Biotreatment of dye-containing pollutants may be an effective method for decontamination owing to its eco-friendliness, low cost, and high efficiency relative to chemical and physical methods (Verma and Madamwar, 2003). Many microorganisms, such as *Aeromonas hydrophila* (Chen *et al.*, 2003), *Escherichia coli* NO_3 (Chang and Kuo, 2000), and *Chlorella* species (Daneshvar *et al.*, 2007b), are capable of decolouring various dyes. Sun *et al.* (2016) found that aromatic dye biodegradation by *Irpex lacteus* CD2 requires radical-mediated oxidative reactions and synergistic enzymes. Additionally, Deng *et al.* (2008) found that *Bacillus cereus* can efficiently degrade a broad spectrum of dyes with high decolourising effects, such as triphenylmethane, anthraquinone, and azo dyes. *Bacillus cereus* strain that can decolorise all three main group dyes efficiently may be useful for bioremediation applications. However, the definite metabolic process and the key enzymes involved in MG degradation by *B. cereus* are still poorly understood.

Proteomic technology is a powerful tool for studies of the global changes in eukaryotic and prokaryotic protein levels and has been used to analyse protein patterns in microorganisms in response to pollutants and environmental stress (Ranish *et al.*, 2003; Liu *et al.*, 2020). iTRAQ-facilitated quantitative proteomics uses an isobaric labelling method and tandem mass spectrometry technology to identify differential protein expression response to various treatments (Zieske, 2006). In this study, we used iTRAQ-facilitated proteomics as a tool to investigate the functional proteins involved in the biodegradation of MG by *B. cereus*. RT-qPCR was also used to confirm the genes involved in the benzoate degradation process. The results of this study provide a comprehensive overview of the proteins involved in the degradation of MG by *B. cereus* and improves our understanding of the molecular mechanisms underlying the biodegradation of MG.

Materials and Methods

Bacterial strain and culture conditions

Bacillus cereus strain ATCC 10987 (genome accession number PRJNA318652) was purchased from ATCC (http://www.atcc.org). *Bacillus cereus* was cultured in 1 g/L NH_4Cl, 3 g/L KH_2PO_4, 12.8 g/L $Na_2HPO_4{\cdot}H_2O$, 0.5 g/L NaCl, and 2 g/L yeast extract with or without MG (> 99% purity; Licai) at 30°C. An initial cell concentration of approximately 0.05 mg/ml was used to inoculate the decolourising medium for subsequent experiments. Cultures grown in non-MG medium were used as controls. The cell growth curves were obtained through measuring the OD560 of the resuspended cell precipitate in PBS after centrifugation. Dye decolourisation was analysed spectrophotometrically by measuring the absorbance of the supernatant from the culture medium at OD616 after centrifugation at 14,000 × *g* for 10 min. The removal effect of MG was calculated as: decolourisation rate= $(A_0 - A_t)/A_0 \times 100\%$, where A_t and A_0 represent the absorbance of the supernatant at cultivation time and at baseline, respectively (Yu and Wen, 2005). Decolourisation rates were analysed in triplicate.

Bacterial quantification

The CFU profiles of *B. cereus* cultured with different MG concentrations were conducted to further demonstrate its potential toxic effects on the cells. Specifically, *B. cereus* was inoculated in the medium with 0, 50, 200, and 400 mg/L of MG. After 10 h, the cultures were transferred into a 96-well plate in triplicates. Then, 10-fold serial dilutions were made 8–10 times with fresh medium and the 10 µl dilutions from the wells were dripped onto the nutrient agar plates. After 10 h grown at 30°C, the colonies were counted.

Sample preparation and concentration test

A flow chart for iTRAQ experiments and functional analysis was shown in Supplementary data Fig. S1. Specifically, the bacterial cells in the logarithmic growth cultured with 200 mg/L of MG were collected by centrifugation at 4°C. Then the precipitates were washed with cold PBS. Cells grown in non-MG medium served as negative controls. Protein samples from six independent biological replicates in control (C) and test (T) treatments were extracted as previous report (Ge *et al.*, 2012) and mixed separately. Each protein sample was prepared in duplicate and tagged as follows: untreated samples were labeled with tags 114 (C_1) and 115 (C_2); MG loading samples were labeled with tags 116 (T_1) and 117 (T_2). Pearson's correlation was used to validate the analytical reproducibility of the two biological replicates for each condition in this study. The protein concentration was monitored using 2-D Quant kit assay reagents (Takara Bio) following the manufacturer's instructions.

Strong cation exchange (SCX) chromatography

The trypsin-digested peptides (100 µg) from the treatment group were signed with iTRAQ reagents (iTRAQ Reagent-4 Multiplex Kit; Applied Biosystems) according to the manufacturer's instructions. Before liquid chromatography-tandem mass spectrometry (LC-MS/MS) analysis, peptides were purified by SCX chromatography as described previously (Adav *et al.*, 2011). A C18 Cartridge (Sigma) and an offline fraction collector were used to desalt and collect the eluted peptides. Then, the collected fractions were dried by vacuum centrifugation for LC-MS/MS analysis.

LC-MS/MS and Mass spectrometric data analyses

Q Exactive Orbitrap mass spectrometer united with an Easy-nLC 1200 System (both from Thermo Fisher Scientific) were used to conduct the LC-MS/MS experiments as previously described (Jia *et al.*, 2017). ProteinPilot Software v4.1 (AB SCIEX) was used to identify and quantify proteins (Xie *et al.*, 2016). The parameters were defined as follows: (i) cysteine alkylation: MMTS; (ii) sample type: iTRAQ 4-plex (peptide-labelled); (iii) special factors: none; (iv) digestion: trypsin; (v) specify processing: quantitate; (vi) species: none; (xii) database: concatenated NCBI RefSeq *B. cereus* (strain ATCC 10987); (xiii) search effort: thorough. Only identified peptides with a false discovery rate (FDR) of 1% or less (Wang *et al.*, 2017) and at least two peptides matched were considered for further analysis. Differentially expressed proteins were identified with a fold-change ≥ 1.5 (increased) or ≤ 0.5 (decreased) and a *p*-values ≤ 0.05 in two biological replicates.

Gene ontology (GO; http://www.geneontology.org/) and KEGG database (http://www.genome.jp/kegg/mapper.html) platforms were used to analyse the functional subcategories and significantly enriched metabolic pathways of differentially regulated proteins, respectively. The most significant pathways were identified with corrected *P*-values of less than 0.05.

Real-time Quantitative PCR

Total RNA was extracted from each culture using TRIzol (Takara). Then, 1 µg of purified RNA sample was reverse transcribed to cDNA using the RevertAid First Strand cDNA Synthesis Kit (Takara). RT-qPCR was carried out using the real-time fluorescence detection method on an Applied Biosystems 7300 system (Applied Biosystems). Specifically, qPCR was set up with a 20 µl reaction volume, containing primer mix: 0.4 µl of each primer (10 µM), 2 × SYBR Green Real Time PCR Master Mix: 10 µl, template cDNA: 1 µl, ddH_2O: 8.2 µl. The PCR condition were as follows: 95°C for 2 min; 95°C for 15 sec, the annealing temperature (Supplementary data Table S1) for 30 sec, 72°C for 25 sec, 40 cycles; followed by a melting curve for 15 sec at 95°C, 60 sec at 60°C, and finally at 95°C for 15 sec. The primer sets used for qPCR were designed using Vector NTI 10 based on the DNA sequences of corresponding genes, and the sequences were listed in Supplementary data Table S1. The $2^{-\Delta\Delta CT}$ method was used to calculate the fold change, relative to the housekeeping gene *gatB* (Reiter *et al.*, 2011).

Results and Discussion

Growth rate and decolourisation efficiency

To examine how MG-loading responses were reflected in changes in the growth rates of *B. cereus*, we evaluated its growth in the presence of various concentrations of MG. Figure 1 summarises the CFU and cell growth profiles of *B.*

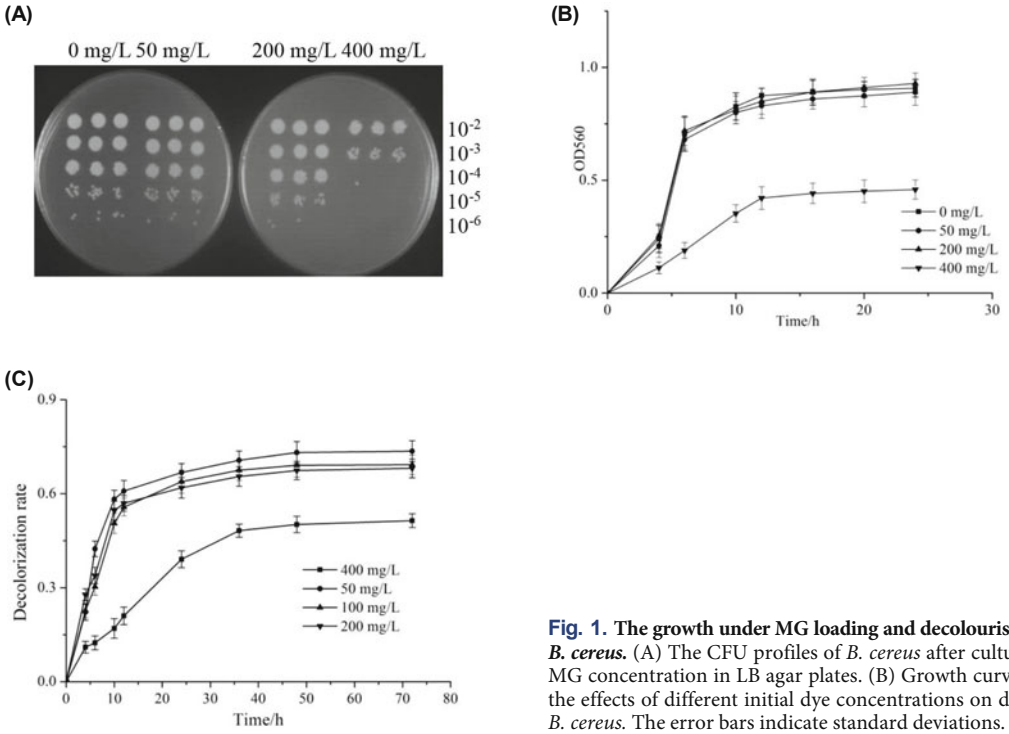

Fig. 1. The growth under MG loading and decolourisation efficiency by *B. cereus*. (A) The CFU profiles of *B. cereus* after cultured with different MG concentration in LB agar plates. (B) Growth curves of *B. cereus* (C) the effects of different initial dye concentrations on decolorization with *B. cereus*. The error bars indicate standard deviations.

cereus in the presence of 50, 200, and 400 mg/L of MG. Culturing of *B. cereus* with various concentrations of MG revealed that at concentrations lower than 400 mg/L of MG, the colony counts of *B. cereus* reached 10^6 CFU/ml and no growth difference was observed among these bacterial cells, as shown in Fig. 1A. However, at a concentration of 400 mg/L of MG, the colony counts of *B. cereus* reached 10^4 CFU/ml. In addition, the growth curve of *B. cereus* under different MG concentrations further corroborated the colony counting results (Fig. 1B). These results suggested that the growth of *B. cereus* was inhibited at high MG concentrations. The growth inhibition of MG in many microorganisms has been verified, such as *Staphylococcus aureus* (Culp and Beland, 1996), *Phanerochaete chrysosporium* (Murugesan *et al.*, 2009), *Bacillus subtilis*, and *Saccharomyces cerevisiae* (Gopinathan *et al.*, 2015). The inhibition effect of MG is attributed to inhibition of bacterial DNA replication and enhanced reactive oxygen species in cells (Culp and Beland, 1996; Gopinathan *et al.*, 2015). In this study, 400 mg/L of MG obviously inhibited the growth of *B. cereus*. Thus, even though MG did not inhibit the growth of *B. cereus* at a low concentration, the bacteria underwent cellular stress and sustained damage from genotoxic and cytotoxic effects of MG to maintain normal growth. As it is important to compare the bacterial proteome at the same phase of culture, the concentration of MG that did not inhibit visible growth of *B. cereus* (200 mg/L) was selected and all the protein samples for iTRAQ analyses were collected at the late log phase by centrifugation.

The decolourisation efficiency of *B. cereus* was analysed in media containing different concentrations of MG. Although the total dye decolourisation decreased sharply when the dye concentration was increased to 400 mg/L (Fig. 1C), the quantity of MG increased with an increase in initial dye concentration. Chen *et al.* (2009) also reported that the amount of removed colour increased when the initial MG concentration was increased. This is probably due to a higher initial concentration of the dye may enhance the driving force to overcome mass transfer resistance of the dye between the cells and MG (Daneshvar *et al.*, 2007a).

Functional classification of proteins quantified by iTRAQ from *B. cereus*

In this study, an iTRAQ-facilitated comparative proteomics approach was used to identify the proteins response involved in the degradation of MG by *B. cereus*. Pearson's correlation was used to validate the analytical reproducibility of the biological replicates (Yang *et al.*, 2016). A 45° diagonal line with little variation was obtained throughout the detection range, indicating that the experiments were highly reproducible (see Supplementary data Fig. S2). In a bioinformatic analysis, 407 differentially regulated proteins with unused protein scores of 1.3 or greater as a threshold value were identified from 1,725 unique peptides (see Supplementary data Table S2). The distributions of length and the number of peptides and sequence coverage for the proteins identified by iTRAQ proteomics are shown in Supplementary data Fig. S3A–C.

Among the 407 differentially expression proteins, 209 were upregulated and 198 proteins were downregulated (iTRAQ ratio ≥ 1.5 or ≤ 0.667; P values of both < 0.05). These regulated proteins were clustered functionally according to cellular components, biological processes, and molecular functions based on a GO analysis, as shown in Fig. 2A–C. Within the three main categories, the largest proportion of the cellular component category was represented by cell part (72.3%) and macromolecular complex (17%); in the biological pro-

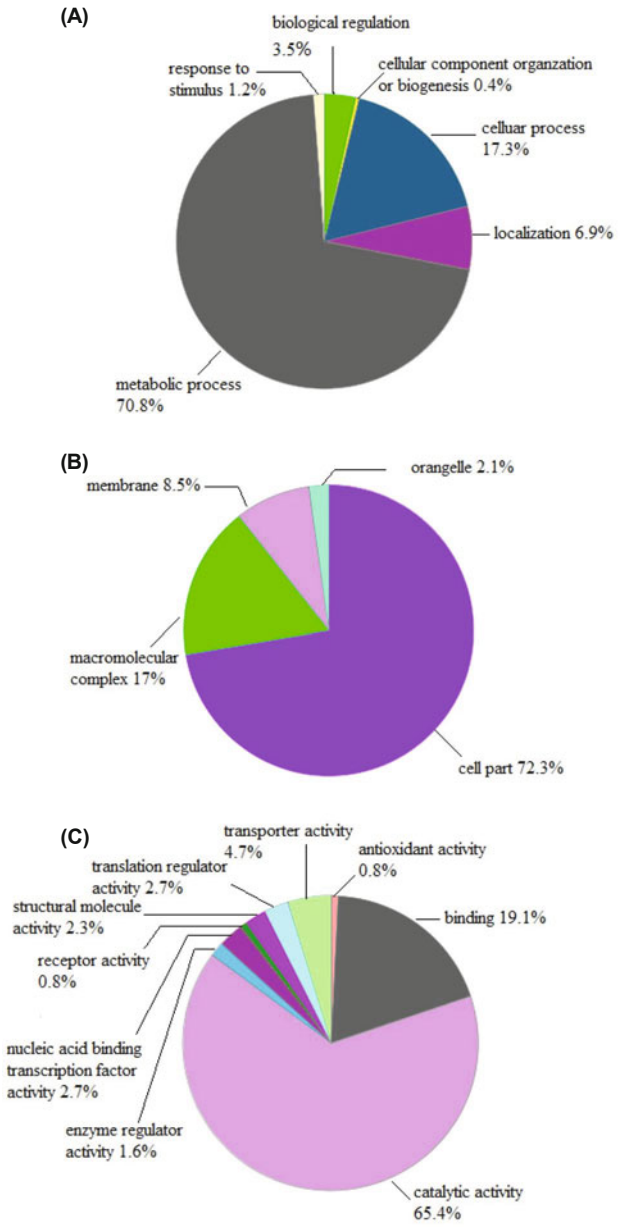

Fig. 2. Gene ontology analysis of differentially expressed proteins of *B. cereus* under MG loading. (A) The altered proteins in biological process category; (B) The altered proteins in cellular components category; (C) The altered proteins in molecular functions category.

cess category, it was the metabolic process (70.8%) and cellular process (17.3%); and in the molecular function category, the proteins were enriched in catalytic activity (65.4%) and binding (19.1%) (Fig. 2). A large number of proteins involved in "metabolic processes" and "catalytic activity" were up- or down-regulated differentially. In addition, proteins involved in "antioxidant activity" and "responses to stimuli" were all up regulated (Fig. 2). In particular, the GO category "metabolic processes" contained 33 up-regulated protein species in the MG loading samples including synthase (PdxS, CarA, CarB, RibH, ArgJ, ArgG, and MiaB), ligase (SucC, SucD, ArgS, and GltX), and H^+-transporting ATPase subunits epsilon and gamma. Furthermore, five dehydrogenases (GuaB, Mdh, GcvPB, PdhA, and RocA) in the category "catalytic activity" were also increased in the MG loading samples, while three dehydrogenases (MtnB, IlvD, and HisD) were decreased. In the category "antioxidant activity", glutathione peroxidase (BsaA), organic hydroperoxide resistance protein (BCE_4559), alkyl hydroperoxide reductase (AhpC and AhpF) were up-regulated 3 to 7 fold. In the category "responses to stimuli", four proteins, including Flavohemoprotein (Hmp), Serine hydroxymethyltransferase (GlyA), ATP-dependent helicase/nuclease subunit A (AddA), and DNA mismatch repair protein (MutS) were all increased. Therefore, MG loading strongly reshaped the *B. cereus* proteome by affecting many aspects of cell physiology, including metabolism, physiological activity, and stress responses.

Pathway analysis

To better understand the effects of MG stress on bacterial pathways, a KEGG pathway analysis (Kanehisa *et al.*, 2008) was performed using the proteins that were down- and up-regulated in response to MG stress (Fig. 3). Under the MG loading, 45 proteins were related to carbon metabolism, such as glycolysis/gluconeogenesis, tricarboxylic acid cycle (TCA), and pyruvate metabolism (Table 1). In comparison, there were 13 down regulated proteins involved in amino acid metabolism and biosynthesis, including valine, leucine, arginine, proline, and isoleucine metabolism in MG-treated *B. cereus* cells. Additionally, proteins involved in other biological processes, such as fatty acid metabolism, peptidoglycan biosynthesis, and pantothenate biosynthesis (Table 1), were down regulated. These results indicated that MG exposure in the form of cellular stress, could affect various metabolic pathways of *B. cereus*, which might explain the inhibitory effect of MG on growth of *B. cereus* at a high concentration. It is worth noting that five up-regulated proteins (UvrA, Mfd, LigA, PcrA, and PolA) related to nucleotide excision repair, indicating that there may have been a DNA damage after MG loading and that proteins related to DNA repair function play a role in MG biodegradation. Thus, the up-regulation of DNA repair proteins might be a protective mechanism that *B. cereus* uses against MG loading, whereas the decrease in specific metabolic flow in response to MG stress may be a comprehensive MG resistance strategy.

Analysis of proteins involved in carbon metabolism and energy metabolism

Proteins related to pyruvate metabolism and TCA exhibited increased expression in the presence of MG in *B. cereus*; these proteins included dihydrolipoyl dehydrogenase, pyruvate dehydrogenase complex, and acetyl-CoA synthetase. Additionally, pyruvate dehydrogenase complex (PDHC), a vital enzyme involved in energy metabolism, showed obvious up regulation in the MG-treated samples. PDHC is a substrate for the TCA. It catalyses pyruvate to acetyl-CoA. This process plays a crucial role in the progression from glycolysis to TCA (Mattevi *et al.*, 1992). In addition, the increases in fructose 1,6-bisphosphatase and pyruvate carboxylase suggest increased gluconeogenesis. Thus, these results suggest that the increased expression of proteins involved in carbon

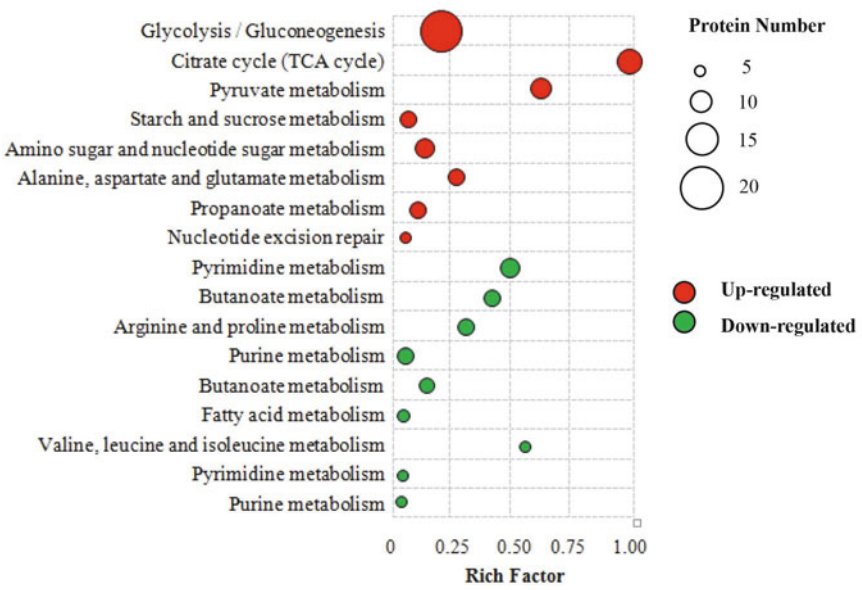

Fig. 3. Pathway classification of differentially expressed proteins of *B. cereus* under MG loading based on KEGG enrichment analysis. Rich factor, the proportion of the number of differentially expressed proteins to the number of total genes in related pathway. Pathways with more than five changed proteins are shown.

metabolism may increase the production of carbon skeletons or indirectly increase the energy supply under MG stress. In addition, three subunits of the ATP synthase complex involved in energy metabolism, ATP synthase subunit beta (AtpC) and ATP synthase gamma chains (AtpH and AtpG), were significantly upregulated. These findings are consistent with the observed upregulation of members of the carbohydrate metabolism pathway in *B. cereus* during MG degradation. Yi *et al.* (2016) found that three subunits of ATP synthase (AtpA, AtpD, and AtpG) showed significantly up regulated expression during the triphenyltin biodegradation process in an engineered strain of *E. coli*. Furthermore, Szewczyk *et al.* (2015) suggested that the increased expression of energy-related proteins appeared to be a general result during the xenobiotic biodegradation process. In this study, the upregulation expression of these three subunits of ATP synthase suggested vigorous energy demands of *B. cereus* during the MG biodegradation process.

Analysis of proteins involved in nucleotide repair and stress response

Of the aforementioned altered proteins, the expression of many nucleotide excision repair proteins increased. This may be due to an intracellular compensation mechanism since MG can bind to almost all available DNA sites and cause bacterial DNA damage (Culp and Beland, 1996). In particular, seven proteins (UvrA, Mfd, LigA, PcrA, MutS, PolA, and DnaX) involved in nucleotide excision repair and mismatch repair were up-regulated 3-8 fold. Among these, UvrA catalyses the recognition and processing of DNA lesions. LigA catalyses the formation of phosphodiester linkages between 5′-phosphoryl and 3′-hydroxyl groups in double-stranded DNA and

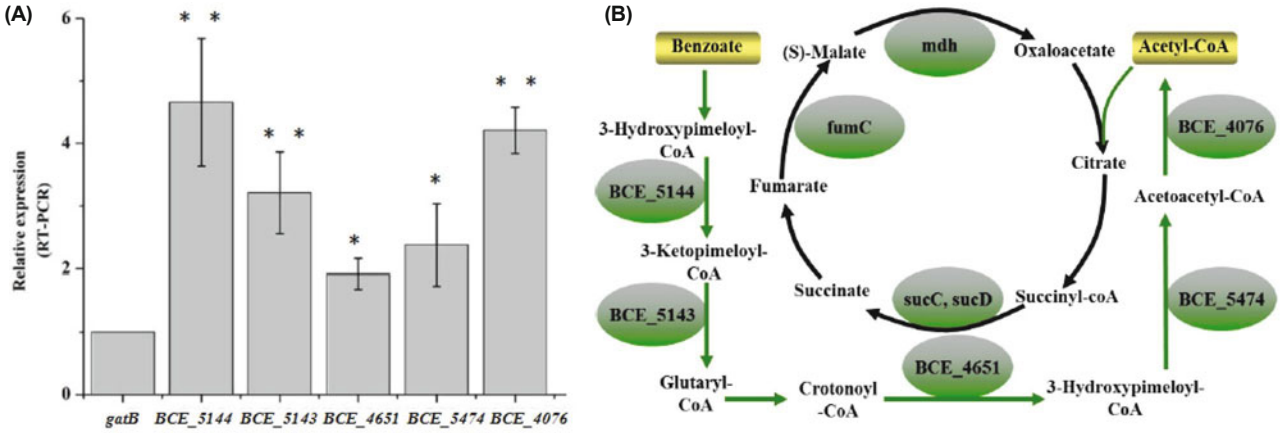

Fig. 4. Benzoate degradation pathway play an important role in the degradation of MG. (A) The transcriptional levels of selected genes associated with benzoate degradation in *B. cereus* under MG loading. Result represents the average of triplicate experiments. Error bars indicate one standard deviation. ** $P < 0.01$; * $P < 0.05$, Student's *t*-test. (B) A pathway model of metabolic flow from benzoate degradation to citrate cycle shown in the KEGG database. Proteins with increased abundance in *B. cereus* upon MG loading are framed in ovals.

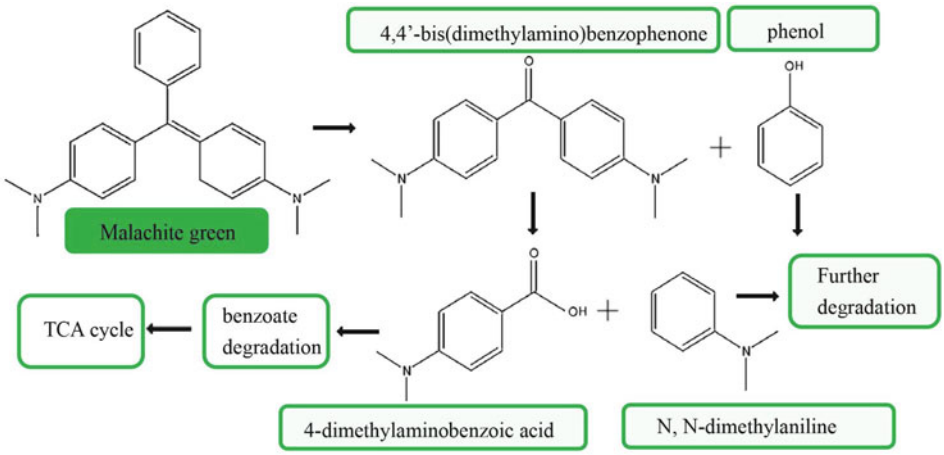

Fig. 5. **The proposed biodegradation pathways of MG by *B. cereus* based on the current proteomics results and previous literatures.**

is essential for DNA replication and repair of damaged DNA. DnaX is responsible for most of the replicative DNA synthesis (Rasko *et al.*, 2004). Flavohemoprotein (Hmp) plays a central role in the inducible response to various noxious nitrogen compounds (Rasko *et al.*, 2004). We found that it was up regulated 1.82 fold in MG loading group. Previously, serine

Table 1. **Part of differentially expressed proteins and their assigned or assumed functions in selected functional categories**

Classification	Protein name	Accession No.	Gene	T:CK[a]	*P*-value[b]
Pyruvate metabolism	Pyruvate dehydrogenase complex E1 component, beta subunit	Q731Z5	*pdhB*	2.77	0.0001
	Pyruvate dehydrogenase complex E2 component	Q731Z6	*pdhC*	2.02	0.0106
	Malate oxidoreductase	Q73AA8	*ykwA*	4.04	0.0002
	Pyruvate carboxylase	Q732C0	*pyc*	3.53	0.0000
	Pyruvate dehydrogenase complex E1 component, alpha subunit	Q731Z4	*pdhA*	3.31	0.0000
TCA cycle	Succinyl-CoA ligase [ADP-forming] subunit beta	Q732N4	*sucC*	6.31	0.0000
	Succinyl-CoA ligase [ADP-forming] subunit alpha	Q732N5	*sucD*	4.96	0.0258
	Fumarate hydratase class II	Q73AD9	*fumC*	4.67	0.0000
	Malate dehydrogenase (TCA)	Q72ZE5	*mdh*	1.76	0.0038
Energy metabolism	ATP synthase subunit delta	Q72XE5	*atpH*	4.92	0.0093
	ATP synthase gamma chain	Q72XE7	*atpG*	3.18	0.0068
	ATP synthase epsilon chain	Q72XE9	*atpC*	2.3	0.0447
Glutathione metabolism	Glutathione peroxidase	Q739E0	*bsaA*	3.21	0.0139
	Aminoacyl-histidine dipeptidase	Q737W8	*Pepd*	4.67	0.0182
	Cytosol aminopeptidase	Q72YG1	*pepA*	3.06	0.0000
Benzoate degradation	3-Hydroxyacyl-CoA dehydrogenase	Q72Y77	*BCE_5144*	20.24	0.0000
	Acetyl-CoA acetyltransferase	Q72Y78	*BCE_5143*	9.46	0.0003
	Enoyl-CoA hydratase	Q72ZL7	*BCE_4651*	2.67	0.0039
	3-Hydroxyacyl-CoA dehydrogenase	Q72XA4	*BCE_5474*	9.44	0.0005
	Acetyl-CoA acetyltransferase	Q731T9	*BCE_4076*	7.14	0.0017
Nucleotide repair	UvrABC system protein A	Q72XV2	*uvrA*	3.28	0.0003
	Transcription repair coupling factor	Q73FF5	*mfd*	2.21	0.0134
	DNA ligase	Q73EM3	*ligA*	2.08	0.0031
	ATP-dependent DNA helicase	Q73EM4	*pcrA*	7.78	0.0035
	DNA polymerase I	Q72ZF0	*polA*	5.91	0.0000
	DNA mismatch repair protein	P61665	*mutS*	8.46	0.0005
	DNA polymerase III subunit gamma/tau	Q73FI6	*dnaX*	1.72	0.0141
Peptidoglycan biosynthesis	D-Alanyl-D-alanine carboxypeptidase	Q731M1	*dacF*	0.02	0.0000
	UDP-N-acetylmuramoylalanine–D-glutamate ligase	Q732F6	*murD*	0.38	0.0022
	Transpeptidase	Q738M4	*BCE_2370*	0.36	0.0246
Pantothenate biosynthesis	Ketol-acid reductoisomerase 1	Q73BA1	*ilvC1*	0.02	0.0021
	Ketol-acid reductoisomerase 2	Q73A47	*ilvC2*	0.02	0.0000
	Dihydroxy-acid dehydratase	Q9XBI3	*ilvD*	0.04	0.0000

[a] The ratio between protein levels in MG-loading (T) and control (CK).
[b] *P*-value, Student's *t*-test.

hydroxymethyltransferase (GlyA) has been reported could elevate the tolerance to the hyperosmosis stress in *E. coli* (Mishra *et al.*, 2019) and it was found to be up-regulated 2.21 fold in 200 mg/L of MG loading group, respectively. Notably, three proteins (DacF, MurD, and BCE_2370) involved in peptidoglycan biosynthesis were down-regulated. The peptidoglycan plays a structural role in the bacterial and counteracting the osmotic pressure (Amera *et al.*, 2020). Therefore, high MG concentration and decreased peptidoglycan biosynthesis may cause osmotic stress to cells, whereas up-regulated GlyA could be a similar pressure response strategy to MG in *B. cereus*.

Analysis of proteins involved in glutathione (GSH) metabolism

Textile dyes as environmental pollutants play a key role in the generation of oxidative stress in cells and hinder the growth of microbes (Rawat *et al.*, 2016). Our results showed that some antioxidant enzymes related to GSH metabolism showed up-regulated expression during MG biodegradation by *B. cereus*, such as glutathione peroxidase, aminoacyl-histidine dipeptidase, and cytosol aminopeptidase. GSH is an important antioxidant in organisms. It can remove redundant active oxygen free radicals and mitigate the damage caused by the peroxidation of membrane lipid during cell metabolism (Musgrave *et al.*, 2013). Previous studies have indicated that GSH plays a critical role in reducing the toxic effect of MG (Debnam *et al.*, 1993). In a recent study, Yildirim *et al.* (2018) also verified that increased levels of GSH, superoxide dismutase, glutathione S-transferase, and glutathione peroxidase in *Gammarus pulex* improve the capability of *Coriolus versicolor* in MG decolourisation. These findings indicated that cells require active antioxidant proteins to resist MG toxicity. The upregulation of proteins involved in GSH metabolism may enhance the ability of *B. cereus* to protect against oxidative stress and promote MG degradation.

Analysis of proteins involved in benzoate degradation

Two important mechanisms have been shown to mediate the degradation of triphenylmethane dyes (Yatome *et al.*, 1993; Cha *et al.*, 2001). *Bacillus cereus* can degrade MG into 4,4′-bis(dimethylamino)benzophenone and another intermediate metabolite phenol (Deng *et al.*, 2008). This process is similar to the degradation of MG by *Micrococcus* sp. strain BD15. In *Micrococcus* sp. strain BD15, 4,4′-bis(dimethylamino)-benzophenone is degraded to N-dimethylaniline and 4-dimethylaminobenzoic acid and is then further converted into other compounds for degradation (Du *et al.*, 2013). In this study, proteins (BCE_5474, BCE_5144, BCE_4651, BCE_4076, and BCE_5143) related to benzoic acid degradation were significantly up-regulated during the MG biodegradation process in *B. cereus*. RT-qPCR was also performed to confirm the gene expression levels of *BCE_4651*, *BCE_5143*, *BCE_5144*, *BCE_4076*, and *BCE_5474* under exposure to 200 mg/L of MG in *B. cereus* (Fig. 4A), and these results were consistent with those of the proteomics results. Both analyses showed that the transcriptional and translational levels of these genes increased significantly during MG degradation by *B. cereus*. Thus, we hypothesised that 4,4′-bis(dimethylamino) benzophenone was transformed to benzoates for further degradation in *B. cereus*. Afterwards, the end-product of benzoate degradation was further degraded via the TCA (Fig. 4B). Zhang *et al.* (2020) also reported that benzoate degradation pathway was enriched in the degradation of dye reactive black 5, which has a complex benzene ring structure. Based on the number and biological functions of the proteins identified above, our findings suggested that the benzoate degradation pathway may play an important role in MG degradation by *B. cereus*.

Based on the current proteomics results and previous literatures, a potential degradation pathway of MG by *B. cereus* was proposed as shown in Fig. 5. The initial step of the biodegradation of MG by *B. cereus* has been verified in different studies (Deng *et al.*, 2008; Wycliffe *et al.*, 2017). MG is oxidised and decomposed into 4,4′-bis(dimethylamino)benzophenone and phenol. The second step of aromatic polymer degradation is the catabolism to the aromatic compound monomer. However, few proteins involved in those processes were up-regulated, which might be associated with the intrinsic high decolourisation of MG by this strain, since crude enzymes from *B. cereus* have exhibited the ability to degrade MG (Wanyonyi *et al.*, 2017). The main up-regulated proteins were involved in the benzoate degradation pathway and TCA pathways in the MG loading treatment. The TCA pathway involved in the MG degradation has been suggested in different strains such as *Pseudomonas*, *Burkholderia* (Zhang *et al.*, 2020). This study proposed that the benzoate degradation pathway may be responsible for further degradation of aromatic compounds from MG. Therefore, the degradation pathway of MG by *B. cereus* proposed in this study provides new insights into the mechanism underlying biodegradation of MG.

Conclusion

In conclusion, our study identified a large group of differentially expressed proteins in *B. cereus* involved in the degradation of MG using iTRAQ-based LC-MS/MS. The differentially expressed proteins are involved in protection against MG stress, promoting bacterial growth, and minimising oxidative stress during MG biodegradation. Additionally, we found the benzoate degradation pathway was enhanced in the MG degradation process. However, further studies are required to construct knockout mutant to verify the gene function involved in MG degradation. These results reveal the first comprehensive proteome of MG biodegradation, providing new insight into the molecular mechanisms underlying MG biodegradation.

Acknowledgments

We thank the National Key Research and Development Program of China (2018YFD0800403), the National Natural Science Foundation of China (No. 21978287), and the Science and Technology Service Network Initiative Project of the Chinese Academy of Sciences (KFJ-STS-QYZX-112) for their financial support.

Conflict of Interest

The authors declare that there is no conflict of interests regarding the publication of this paper.

References

Adav, S.S., Ng, C.S., and Sze, S.K. 2011. iTRAQ-based quantitative proteomic analysis of *Thermobifida fusca* reveals metabolic pathways of cellulose utilization. *J. Proteomics* **74**, 2112–2122.

Amera, G.M., Khan, R.J., Pathak, A., Jha, R.K., Muthukumaran, J., and Singh, A.K. 2020. Computer aided ligand based screening for identification of promising molecules against enzymes involved in peptidoglycan biosynthetic pathway from *Acinetobacter baumannii*. *Microb. Pathog.* **147**, 104205.

Cha, C.J., Doerge, D.R., and Cerniglia, C.E. 2001. Biotransformation of malachite green by the fungus *Cunninghamella elegans*. *Appl. Environ. Microbiol.* **67**, 4358–4360.

Chang, J.S. and Kuo, T.S. 2000. Kinetics of bacterial decolorization of azo dye with *Escherichia coli* NO_3. *Bioresour. Technol.* **75**, 107–111.

Chen, C.Y., Kuo, J.T., Cheng, C.Y., Huang, Y.T., Ho, I.H., and Chung, Y.C. 2009. Biological decolorization of dye solution containing malachite green by *Pandoraea pulmonicola* YC32 using a batch and continuous system. *J. Hazard. Mater.* **172**, 1439–1445.

Chen, K.C., Wu, J.Y., Liou, D.J., and Hwang, S.C.J. 2003. Decolorization of the textile dyes by newly isolated bacterial strains. *J. Biotechnol.* **101**, 57–68.

Culp, S.J. and Beland, F.A. 1996. Malachite green: A toxicological review. *J. Am. Coll. Toxicol.* **15**, 219–238.

Daneshvar, N., Ayazloo, M., Khataee, A.R., and Pourhassan, M. 2007a. Biological decolorization of dye solution containing malachite green by microalgae *Cosmarium* sp. *Bioresour. Technol.* **98**, 1176–1182.

Daneshvar, N., Khataee, A.R., Rasoulifard, M.H., and Pourhassan, M. 2007b. Biodegradation of dye solution containing malachite green: optimization of effective parameters using taguchi method. *J. Hazard. Mater.* **143**, 214–219.

Debnam, P., Glanville, S., and Clark, A.G. 1993. Inhibition of glutathione *s*-transferases from rat liver by basic triphenylmethane dyes. *Biochem. Pharmacol.* **45**, 1227–1233.

Deng, D., Guo, J., Zeng, G., and Sun, G. 2008. Decolorization of anthraquinone, triphenylmethane and azo dyes by a new isolated *Bacillus cereus* strain DC11. *Int. Biodeterior. Biodegradation* **62**, 263–269.

Du, L.N., Zhao, M., Li, G., Xu, F.C., Chen, W.H., and Zhao, Y.H. 2013. Biodegradation of malachite green by *Micrococcus* sp. strain BD15: Biodegradation pathway and enzyme analysis. *Int. Biodeterior. Biodegradation* **78**, 108–116.

Fessard, V., Godard, T., Huet, S., Mourot, A., and Poul, J.M. 1999. Mutagenicity of malachite green and leucomalachite green in *in vitro* tests. *J. Appl. Toxicol.* **19**, 421–430.

Ge, P., Ma, C., Wang, S., Gao, L., Li, X., Guo, G., Ma, W., and Yan, Y. 2012. Comparative proteomic analysis of grain development in two spring wheat varieties under drought stress. *Anal. Bioanal. Chem.* **402**, 1297–1313.

Gopinathan, R., Kanhere, J., and Banerjee, J. 2015. Effect of malachite green toxicity on non target soil organisms. *Chemosphere* **120**, 637–644.

Henderson, A.L., Schmitt, T.C., Heinze, T.M., and Cerniglia, C.E. 1997. Reduction of malachite green to leucomalachite green by intestinal bacteria. *Appl. Environ. Microbiol.* **63**, 4099–4101.

Jia, D., Wang, B., Li, X., Peng, W., Zhou, J., Tan, H., Tang, J., Huang, Z., Tan, W., Gan, B., *et al.* 2017. Proteomic analysis revealed the fruiting-body protein profile of *Auricularia polytricha*. *Curr. Microbiol.* **74**, 943–951.

Kanehisa, M., Araki, M., Goto, S., Hattori, M., Hirakawa, M., Itoh, M., Katayama, T., Kawashima, S., Okuda, S., Tokimatsu, T., *et al.* 2008. KEGG for linking genomes to life and the environment. *Nucleic Acids Res.* **36**, D480–D484.

Liu, S., Ma, Y., Zheng, Y., Zhao, W., Zhao, X., Luo, T., Zhang, J., and Yang, Z. 2020. Cold-stress response of probiotic *Lactobacillus plantarum* K25 by iTRAQ proteomic analysis. *J. Microbiol. Biotechnol.* **30**, 187–195.

Mattevi, A., de Kok, A., and Perham, R.N. 1992. The pyruvate dehydrogenase multienzyme complex. *Curr. Opin. Struct. Biol.* **2**, 877–887.

Mishra, P., Jain, A., Takabe, T., Tanaka, Y., Negi, M., Singh, N., Jain, N., Mishra, V., Maniraj, R., Krishnamurthy, S.L., *et al.* 2019. Heterologous expression of serine hydroxymethyltransferase-3 from rice confers tolerance to salinity stress in *E. coli* and arabidopsis. *Front. Plant Sci.* **10**, 217.

Moumeni, O. and Hamdaoui, O. 2012. Intensification of sonochemical degradation of malachite green by *Bromide ions*. *Ultrason. Sonochem*. **19**, 404–409.

Murugesan, K., Yang, I.H., Kim, Y.M., Jeon, J.R., and Chang, Y.S. 2009. Enhanced transformation of malachite green by laccase of *Ganoderma lucidum* in the presence of natural phenolic compounds. *Appl. Microbiol. Biotechnol.* **82**, 341–350.

Musgrave, W.B., Yi, H., Kline, D., Cameron, J.C., Wignes, J., Dey, S., Pakrasi, H.B., and Jez, J.M. 2013. Probing the origins of glutathione biosynthesis through biochemical analysis of glutamate-cysteine ligase and glutathione synthetase from a model photosynthetic prokaryote. *Biochem. J.* **450**, 63–72.

Ranish, J.A., Yi, E.C., Leslie, D.M., Purvine, S.O., Goodlett, D.R., Eng, J., and Aebersold, R. 2003. The study of macromolecular complexes by quantitative proteomics. *Nat. Genet.* **33**, 349–355.

Rasko, D.A., Ravel, J., Økstad, O.A., Helgason, E., Cer, R.Z., Jiang, L., Shores, K.A., Fouts, D.E., Tourasse, N.J., Angiuoli, S.V., *et al.* 2004. The genome sequence of *Bacillus cereus* ATCC 10987 reveals metabolic adaptations and a large plasmid related to *Bacillus anthracis* pXO1. *Nucleic Acids Res.* **32**, 977–988.

Rawat, D., Mishra, V., and Sharma, R.S. 2016. Detoxification of azo dyes in the context of environmental processes. *Chemosphere* **155**, 591–605.

Reiter, L., Kolstø, A.B., and Piehler, A.P. 2011. Reference genes for quantitative, reverse-transcription PCR in *Bacillus cereus* group strains throughout the bacterial life cycle. *J. Microbiol. Methods* **86**, 210–217.

Saha, S., Wang, J.M., and Pal, A. 2012. Nano silver impregnation on commercial TiO_2 and a comparative photocatalytic account to degrade malachite green. *Sep. Purif. Technol.* **89**, 147–159.

Srivastava, S., Sinha, R., and Roy, D. 2004. Toxicological effects of malachite green. *Aquat. Toxicol.* **66**, 319–329.

Sun, S., Xie, S., Chen, H., Cheng, Y., Shi, Y., Qin, X., Dai, S.Y., Zhang, X., and Yuan, J.S. 2016. Genomic and molecular mechanisms for efficient biodegradation of aromatic dye. *J. Hazard. Mater.* **302**, 286–295.

Szewczyk, R., Soboń, A., Słaba, M., and Długoński, J. 2015. Mechanism study of alachlor biodegradation by *Paecilomyces marquandii* with proteomic and metabolomic methods. *J. Hazard. Mater.* **291**, 52–64.

Verma, P. and Madamwar, D. 2003. Decolourization of synthetic dyes by a newly isolated strain of *Serratia marcescens*. *World J. Microbiol. Biotechnol.* **19**, 615–618.

Wang, B., Chen, Z., Meng, X., Li, M., Yang, X., and Zhang, C. 2017. iTRAQ quantitative proteomic study in patients with thoracic ossification of the ligamentum flavum. *Biochem. Biophys. Res. Commun.* **487**, 834–839.

Wanyonyi, W.C., Onyari, J.M., Shiundu, P.M., and Mulaa, F.J. 2017. Biodegradation and detoxification of malachite green dye using novel enzymes from *Bacillus cereus* strain KM201428: kinetic and

metabolite analysis. *Energy Procedia* **119**, 38–51.
Xie, H., Yang, D.H., Yao, H., Bai, G., Zhang, Y.H., and Xiao, B.G. 2016. iTRAQ-based quantitative proteomic analysis reveals proteomic changes in leaves of cultivated tobacco (*Nicotiana tabacum*) in response to drought stress. *Biochem. Biophys. Res. Commun.* **469**, 768–775.
Yang, X., Zhang, Z., Gu, T., Dong, M., Peng, Q., Bai, L., and Li, Y. 2016. Data for iTRAQ-based quantitative proteomics analysis of different biotypes in *Echinochloa crus-galli* with multi-herbicide treatment. *Data Brief* **9**, 741–745.
Yatome, C., Yamada, S., Ogawa, T., and Matsui, M. 1993. Degradation of crystal violet by *Nocardia corallina*. *Appl. Microbiol. Biotechnol.* **38**, 565–569.
Yi, W., Yang, K., Ye, J., Long, Y., Ke, J., and Ou, H. 2016. Triphenyltin degradation and proteomic response by an engineered *Escherichia coli* expressing cytochrome P450 enzyme. *Ecotoxicol. Environ. Saf.* **137**, 29–34.
Yildirim, N.C., Tanyol, M., Yildirim, N., Serdar, O., and Tatar, S. 2018. Biochemical responses of *Gammarus pulex* to malachite green solutions decolorized by *Coriolus versicolor* as a biosorbent under batch adsorption conditions optimized with response surface methodology. *Ecotoxicol. Environ. Saf.* **156**, 41–47.
Yu, Z. and Wen, X. 2005. Screening and identification of yeasts for decolorizing synthetic dyes in industrial wastewater. *Int. Biodeterior. Biodegradation* **56**, 109–114.
Zhang, Q., Xie, X., Liu, Y., Zheng, X., Wang, Y., Cong, J., Yu, C., Liu, N., Sand, W., and Liu, J. 2020. Co-metabolic degradation of refractory dye: a metagenomic and metaproteomic study. *Environ. Pollut.* **256**, 113456.
Zhang, C., Zhang, S., Diao, H., Zhao, H., Zhu, X., Lu, F., and Lu, Z. 2013. Purification and characterization of a temperature- and pH-stable laccase from the spores of *Bacillus vallismortis* fmb-103 and its application in the degradation of malachite green. *J. Agric. Food Chem.* **61**, 5468–5473.
Zieske, L.R. 2006. A perspective on the use of iTRAQ reagent technology for protein complex and profiling studies. *J. Exp. Bot.* **57**, 1501–1508.